Influence of sintering atmosphere on the microstructure and water durability of SnO–MgO–P$_2$O$_5$ glass

Jiin-Jyh Shyu · Chih-Hsien Yeh

Abstract Effects of sintering atmosphere (Ar, air, and O$_2$) on the sinterability and crystallization at 380–470 °C of 60SnO, 10MgO, 30P$_2$O$_5$ (mol%) glass powder, and the water durability of the sintered glass were investigated. Increasing the oxygen partial pressure (P_{O_2}) in the sintering atmosphere enhanced the oxidation tendency of Sn^{2+} to Sn^{4+} near the surface region of the glass particles. Therefore, the glass viscosity was increased, resulting in the increase in both the temperature of densification and the temperature at which crystalline phases developed. Phase assemblage and the amounts of crystalline phases were also affected by P_{O_2}. The water durability of the sintered glasses is discussed in terms of the above microstructural parameters.

Introduction

In comparison with silicate glasses, phosphate glasses have low softening temperatures, high thermal expansion, and unique optical characteristics. Thus, low-melting phosphate glasses are candidate materials for applications such as molding glasses [1], laser glasses/fiber lasers [2], optical glasses [3], low-temperature hosts for nuclear waste [4], and soldering/sealing glasses [5–7]. From the environment viewpoint, lead-free, P$_2$O$_5$-based glasses are also alternatives to the PbO-containing glasses [6, 8]. In the past, the practice use of low-melting phosphate glasses is limited due to their relatively poor chemical durability [9, 10]. Several efforts have been made to improve the chemical

durability while retain the low softening temperature of phosphate glasses [6, 9–14]. It has been shown that partial substitution of nitrogen for oxygen in glass structure during melting process is able to improve the chemical durability of phosphate glasses [15–17]. It is also reported that addition of one or more oxides, such as SnO, SiO$_2$, Al$_2$O$_3$, PbO, PbF$_2$, or B$_2$O$_3$, can remarkably improve the chemical durability of phosphate glasses [9, 18–22]. Sn–P–O–F glasses with ultra-low glass transition temperatures, good chemical durability, and relatively high thermal expansion have been reported [9, 23, 24]. Morena [6, 25–27], Yamanaka [28], and Taketami [29] reported that SnO–ZnO–P$_2$O$_5$ glasses have low softening temperature and good chemical durability. We recently published a new glass system SnO–MgO–P$_2$O$_5$ that has low softening temperatures and good chemical durability [30, 31]. Effects of glass composition on the glass formation, thermal properties, and water durability of the cast glasses have been investigated [30]. We also studied the sintering, crystallization, and the resulting properties of the 60SnO, 10MgO, 30P$_2$O$_5$ (mol%) glass in powder form [31].

Several studies on SnO-containing glasses [32–37] indicate that a small amount of Sn^{4+} coexists with Sn^{2+} ions in the glass structure, even if the raw materials for tin contain only Sn^{2+} ions. The Sn^{4+}/Sn^{2+} ratio depends on raw materials, glass composition, and melting conditions, etc. The contamination of tin near the surface of soda–lime–silica float glass has also been studied [38–41], showing that Sn^{2+} and Sn^{4+} coexist and that heat treatment at, e.g., 740 °C, causes the oxidation of Sn^{2+} into Sn^{4+} [39, 40]. According to our previous studies [30, 31], to avoid serious oxidation of Sn^{2+} to Sn^{4+} during melting the SnO–MgO–P$_2$O$_5$ glasses addition of around 1 wt% of sugar and a nitrogen atmosphere are necessary. To the best of the authors, knowledge, no studies focus on the effect of

J.-J. Shyu (✉) · C.-H. Yeh
Department of Materials Engineering, Tatung University,
Taipei 104, Taiwan
e-mail: jjshyu@ttu.edu.tw

oxidation of Sn^{2+} to Sn^{4+} near the surface region of the glass particles during sintering below 500 °C on the microstructure and properties of $SnO–P_2O_5$-based sealing glasses. In this article, effects of sintering atmosphere (Ar, air, and O_2) on the sinterability, crystallization, and water durability of $SnO–MgO–P_2O_5$ glass powder were investigated.

Experimental procedures

Sample preparation

Glass with a nominal composition of 60SnO, 10MgO, and 30P_2O_5 (mol%) was prepared from reagent-grade $Sn_2P_2O_7$ and MgO. The MgO powder was obtained by calcining $Mg(OH)_2$ powder at 700 °C for 1 h. Well-mixed powder containing these chemicals and 1 wt% of sugar was placed in an alumina crucible. The batch was then placed in a furnace at 950 °C in a nitrogen atmosphere. The combination of nitrogen and sugar produced a reducing atmosphere during melting, inhibiting the oxidation of Sn^{2+} to Sn^{4+}. After heating for 15 min, the melt was quenched in deionized water to form glass frits. The dried frits were crushed in an alumina-lined mortar grinder (model RMO, F. Kurt Retsch GmbH & Co. KG, Haan, Germany), and then sieved to obtain a glass powder with particle sizes ranging from 37 to 44 μm.

This glass powder was uniaxially pressed in a steel die to yield disk-shaped samples with a diameter of 5 mm and thickness 3.5 ± 0.05 mm. The green compacts were then placed on soda–lime–silicate glass substrates. The sintered bodies were formed by heating at a rate of 10 °C/min to 380–470 °C and held for 20 min, then furnace cooled (Fig. 1). Atmospheres of Ar, air, and O_2 were applied during the sintering process.

Characterization

The crystallization temperature and weight loss of the glass powder during heating from room temperature to 500 °C
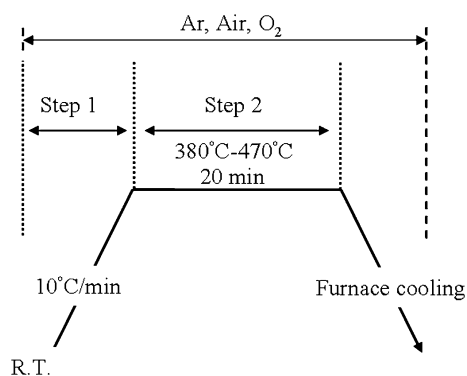

Fig. 1 Sintering conditions for the samples

was measured by differential thermal analysis (DTA, model SDT 2960, TA Instruments, New Castle, DE, USA) and thermogravimetric analysis (TGA, model TGA 2950, TA Instruments), respectively, at a heating rate of 10 K/min. The shrinkage curve of the glass powder compact was measured by thermomechanical analysis (TMA, model Setsys-1750, Setaram Inc., France), using fused quartz as a push rod and a heating rate of 10 K/min. Flowing Ar, air, and O_2 (100 mL/min) were applied during the above thermal analyses. Phase identification of the sintered samples was conducted by X-ray diffraction (XRD) analysis. Measurements were performed on a diffractometer (model X'Pert PRO, PANalytical B.V., Almelo, Netherlands) with Cu K_α radiation. The operating power was 40 kV and 45 mA. A sampling time of 1 s for each interval of 0.02° (2θ) was used. The as-sintered and cross-sectional surfaces of sintered samples were coated with a thin film of gold for scanning electron microscopy (SEM, model JSM-5600, Jeol, Tokyo, Japan) observations. The bottom surface of the sintered sample was less influenced by the sintering atmosphere due to the attachment of the substrate. Therefore, in the water durability test, the bottom surface of the specimen was smeared with epoxy to avoid water attack. The samples were placed in covered polypropylene flasks containing 100 mL of deionized water at 40 °C for 540 min. At least three samples were used for each sintering condition. Finally, the average dissolution rate, defined as the weight loss per unit surface area per unit time, was calculated.

Results and discussion

Thermal analysis of the glass powder

In our previous study [31], the chemical analysis of the 60SnO, 10MgO, 30P_2O_5 (mol%) glass melting at 950 °C for 15 min show that the glass composition consists of 59.40SnO, 10.31MgO, 29.04P_2O_5, and 1.24Al_2O_3 (mol%). Figure 2a shows the original TGA thermograms of the glass powders heated in various atmospheres. The weight loss at lower and higher temperatures may be due to water evaporation and trace evaporation of the glass, respectively. The sequence of weight loss of the glass powder was Ar > air > O_2. Because heating the glass in Ar should not cause oxidation of Sn^{2+}, the actual weight loss curves for air and O_2 can be obtained by subtract the Ar curve from the original curves, as shown in Fig. 2b. It can be seen that the weight gain increased with increasing oxygen partial pressure (P_{O_2}), implying that on the glass particle surfaces the oxidation tendency of Sn^{2+} to Sn^{4+} became more obvious. Ehrt [42] has studied the thermal properties of 60SnO–40P_2O_5 (mol%) melted at 1200 °C for 120 min. She found that the sample was stable up to 1000 °C
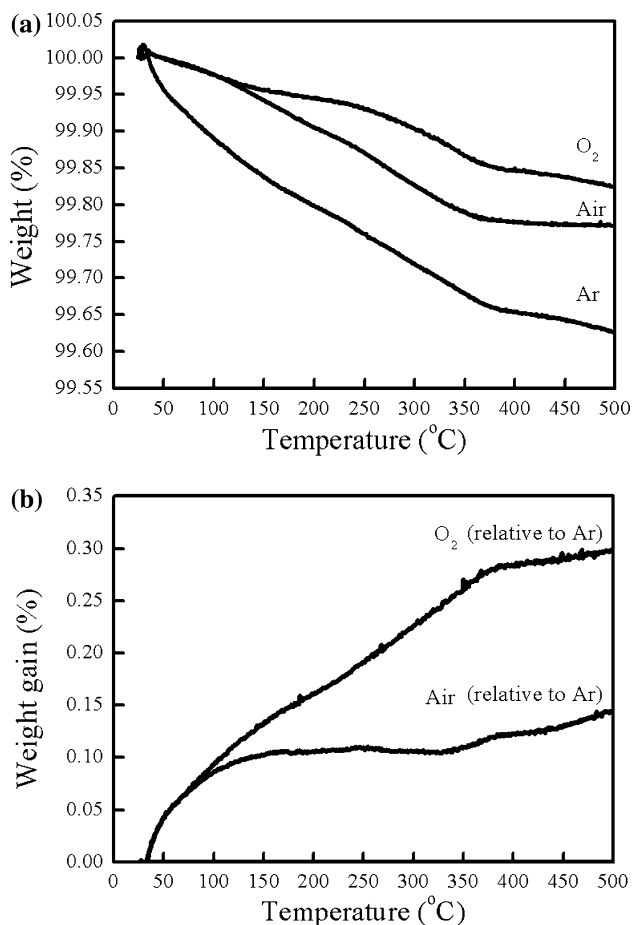
Fig. 2 TGA curves of the glass powders heated in various atmospheres: **a** original data and **b** reduced data
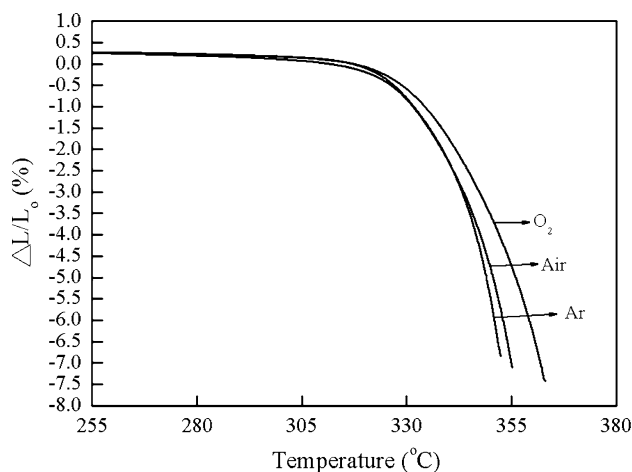

Fig. 3 Shrinkage curves of the glass powder compacts heated in various atmospheres

phosphates, respectively. Moreover, the lower-temperature exothermic peak shifted to a higher temperature with increasing P_{O_2}. On the other hand, the higher-temperature exothermic peak first slightly shifted to a lower temperature, and then moved to a higher temperature.

According to the TGA thermograms in Fig. 2, on the glass particle surfaces the oxidation tendency of Sn^{2+} to Sn^{4+} was significantly enhanced by increasing P_{O_2}. The stronger Sn^{4+}–O bond than the Sn^{2+}–O bond [39] would increase the viscosity of the glass on the particle surfaces. In general, densification of glass is accomplished by viscous-flow sintering mechanism [44]. Therefore, both the sintering temperature (Fig. 3) and the temperature at which crystalline phases developed (Fig. 4) are increased.
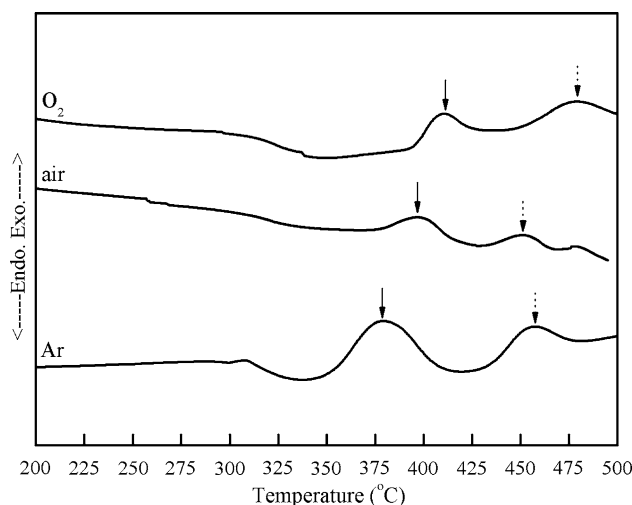
without change of the mass under Ar, while slight increases in the mass could be observed in air atmosphere >600 °C which should be due to the oxidation of Sn^{2+}. Muñoz et al. [43] have studied the oxidation of nitrided Li_2O–Na_2O–PbO–P_2O_5 glass powders below 500 °C and found that the oxidation proceeds first from a surface oxidation, followed by a bulk oxidation controlled by diffusion.

Figure 3 shows the TMA shrinkage curves of the glass powder compacts heated in various atmospheres. The rate of viscous-flow sintering (represented by the curve slope) of the glass powders decreased with increasing P_{O_2}. Figure 4 shows the DTA thermograms of the glass powders heated in various atmospheres. For each curve, two exothermic peaks appeared at a lower temperature (380, 398, and 410 °C for Ar, air, and O_2, respectively) and a higher temperature (457, 451, and 481 °C for Ar, air, and O_2, respectively), indicating that at least two crystalline phases formed during heating. According to the XRD and SEM analyses (described latter in the following section), the lower- and higher-temperature exothermic peaks are associated with the formation of Mg- and Sn-bearing

Fig. 4 DTA curves of the glass powders heated in various atmospheres

Crystalline phase formation and microstructure development

Figure 5a–i shows the as-sintered surfaces of the samples. For the samples sintered at 380 and 410 °C (Fig. 5a–c and d–f, respectively), the surface porosity (or surface roughness) increased with increasing P_{O_2}. For the samples sintered at 470 °C (Fig. 5g–i), the surface porosity is very high for all samples. Figure 6a shows the XRD patterns of the as-sintered surfaces. Although crystalline signals can be detected around 380 °C on the DTA thermograms (Fig. 4), the as-sintered surfaces at 380 °C were X-ray amorphous, suggesting that the amount of crystalline phase is too low to be detected. For the samples sintered at 410 °C, $Mg_3(PO_4)_2$ and $Sn_3(PO_4)_2$ phases (denoted as M_3P and S_3P, respectively) began to appear on the sample surface. After sintering at 470 °C, in addition to the above-mentioned crystalline phases, α-$Mg_2P_2O_7$ (denoted as α-M_2P) also developed. Figure 7 shows the XRD pattern for as-sintered surface of the samples sintered at 470 °C for a prolonged period of time (120 min) in O_2. The S_3P, α-M_2P, $Sn_{2.5}P_3O_{12}$ (ICDD No. 52-1536 which is the most likely), and an unknown phase were formed on the as-sintered surface. It is noted that Sn^{4+} (major) and Sn^{2+} (minor) ions coexist in the $Sn_{2.5}P_3O_{12}$ compound, according to Berry and Thied [45]. From the result of 470 °C/120 min that a

Sn^{4+} containing compound is found, it is suggested that the oxidation of Sn^{2+} to Sn^{4+} should occur at 470 °C for 20 min. Moreover, as shown in Fig. 6a, the total amount of crystalline phases decreased with increasing P_{O_2} for samples sintered at 410 and 470 °C, which matches the DTA results. According to these experimental results, P_{O_2} obviously affected both the assemblage and the amounts of crystalline phases developed on the as-sintered surface. Moreover, according to our previous study [31], the development of S_3P phase remarkably reduced the water durability of the SnO–MgO–P_2O_5 glass. This study shows that increasing P_{O_2} inhibited the development of the S_3P phase.

Figure 8a–i shows the cross-sectional micrographs of the samples. The internal porosity for samples sintered at 380 °C (Fig. 8a–c) and 410 °C (Fig. 8d–f) increased with the increasing P_{O_2}. This effect of P_{O_2} on densification in the sample interior is similar to that on the as-sintered surface (Fig. 5a–c and d–f for 380 and 410 °C, respectively). The internal porosity for samples sintered at 470 °C (Fig. 8g–i) shows no obvious difference with the change in P_{O_2}. For the same sintering atmosphere, the internal porosity decreased reasonably with the increasing sintering temperature. With regard to crystallizability, at 380 °C (Fig. 8a–c) and 410 °C (Fig. 8d–f), only a few of crystalline particles developed (indicated by the arrow) and the
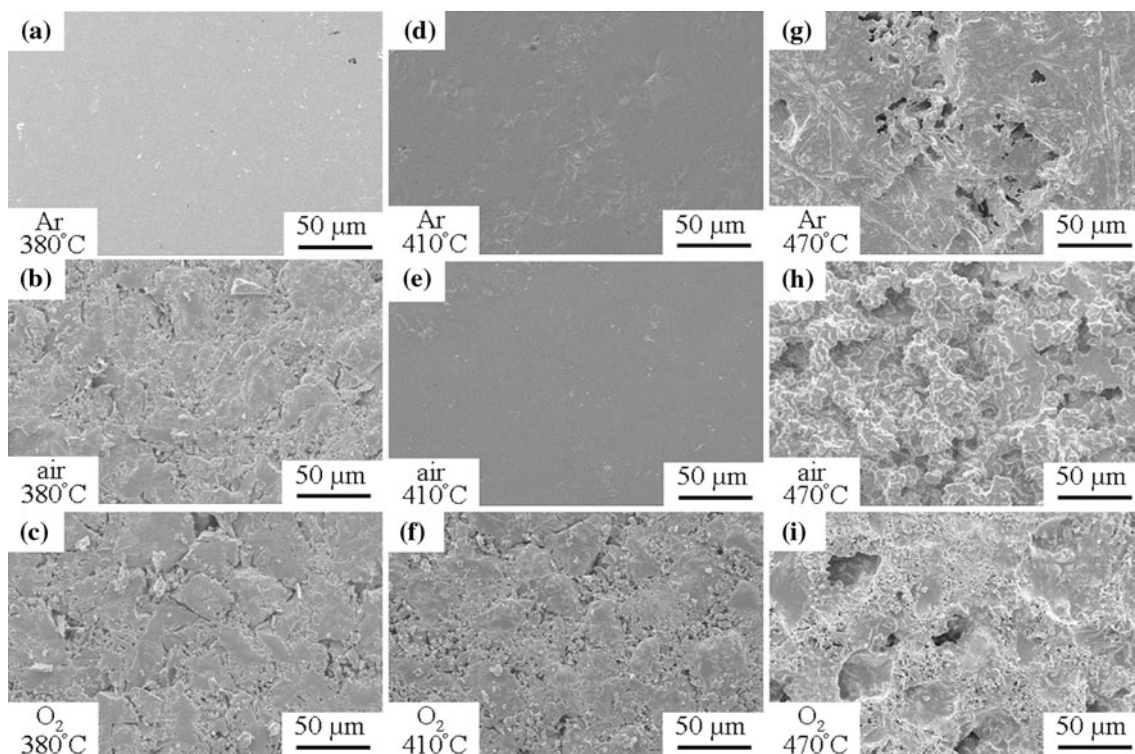

Fig. 5 As-sintered surface micrographs of the samples sintered at 380–470 °C for 20 min in various atmospheres

Fig. 7 XRD patterns for as-sintered surface of the samples sintered at 470 °C for 120 min in O_2 atmosphere (*filled square* $Sn_3(PO_4)_2$, *open triangle* $Sn_{2.5}P_3O_{12}$, # α-$Mg_2P_2O_7$, and ? unknown)
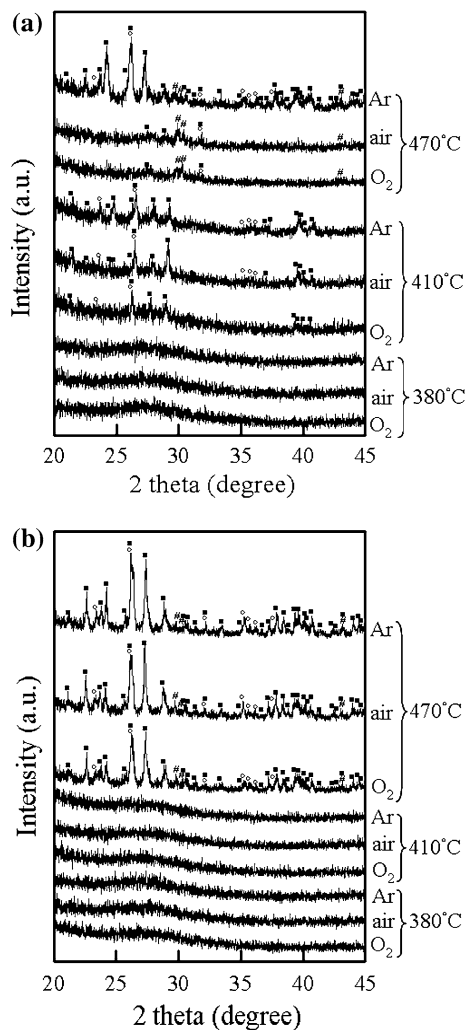
Fig. 6 XRD patterns for **a** as-sintered surface and **b** polished surface of the samples sintered at 380–470 °C for 20 min in various atmospheres (*open circle* $Mg_3(PO_4)$, *filled square* $Sn_3(PO_4)_2$, and # α-$Mg_2P_2O_7$)

corresponding XRD patterns (Fig. 6b) were still amorphous in nature. This reduced crystallization tendency of the sample interior relative to the sample surface was possibly due to the lower tendency to heterogeneous nucleation of the sample interior. When the sintering temperature was increased to 470 °C (Fig. 8g–i), M_3P/M_2P (the dark crystalline particles) and S_3P (the white elongated shaped phase) developed in all three atmospheres, identified with the aids of XRD (Fig. 6b) and EDS analyses. It is also noted that for the same sintering temperature the as-sintered surfaces show obvious difference in XRD patterns (Fig. 6a), while the interior regions show similar XRD patterns (Fig. 6b). This result implies that the externally imposed atmosphere had less influence on the interior than the surface. Similar to that observed with the as-sintered surface (Fig. 6a), the amount of crystalline phases decreased with increasing P_{O_2} (Fig. 6b).
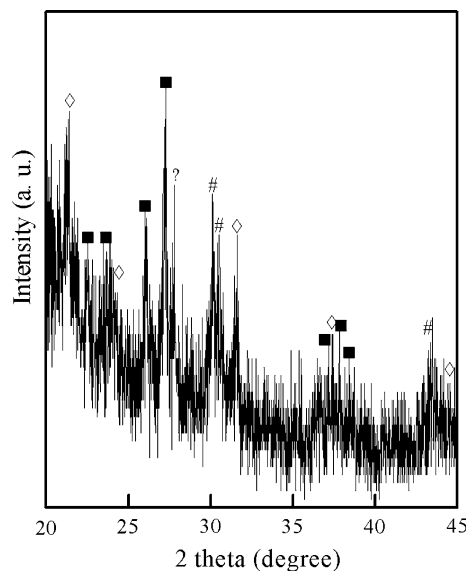
According to the above-described results from thermal analyses, microstructure examination, and XRD, it is summarized that increasing P_{O_2} caused an increase in the oxidation tendency of Sn^{2+} to Sn^{4+}, which increased the viscosity of glass, thus reducing the sinterability and crystallization tendency of both the surface- and the internal-regions of the sample. It is also suggested that the surface- and, at least in the initial stage of sintering, the interior-regions of the samples were both affected by the atmosphere during sintering. Table 1 summarizes the degree of densification and phase assemblage on the sample surface. In the following section, we will prove that the water durability of the sintered glass is determined by these sintering-atmosphere-dependent characteristics.

Water durability

Figure 9 shows the variations in the average dissolution rate, DR, of the sintered samples immersed in 40 °C water for 540 min. For the 380 °C-sintered samples, the DR increased with increasing P_{O_2}. This result can be attributed to the increase in the porosity on the as-sintered surface (Fig. 5a–c) which increases the effective contact-area between glass and water. For the 410 °C-sintered samples, the DR initially decreased slightly with increasing P_{O_2}, and then increased obviously. The reason for this DR decrease may be due to the reduced amount of S_3P phase (Fig. 8a), which has an intrinsically poor water durability. The reason for this DR increase is the increase in surface porosity (Fig. 5d–f). When the sintering temperature was increased to 470 °C, with the increasing P_{O_2} the DR decreased
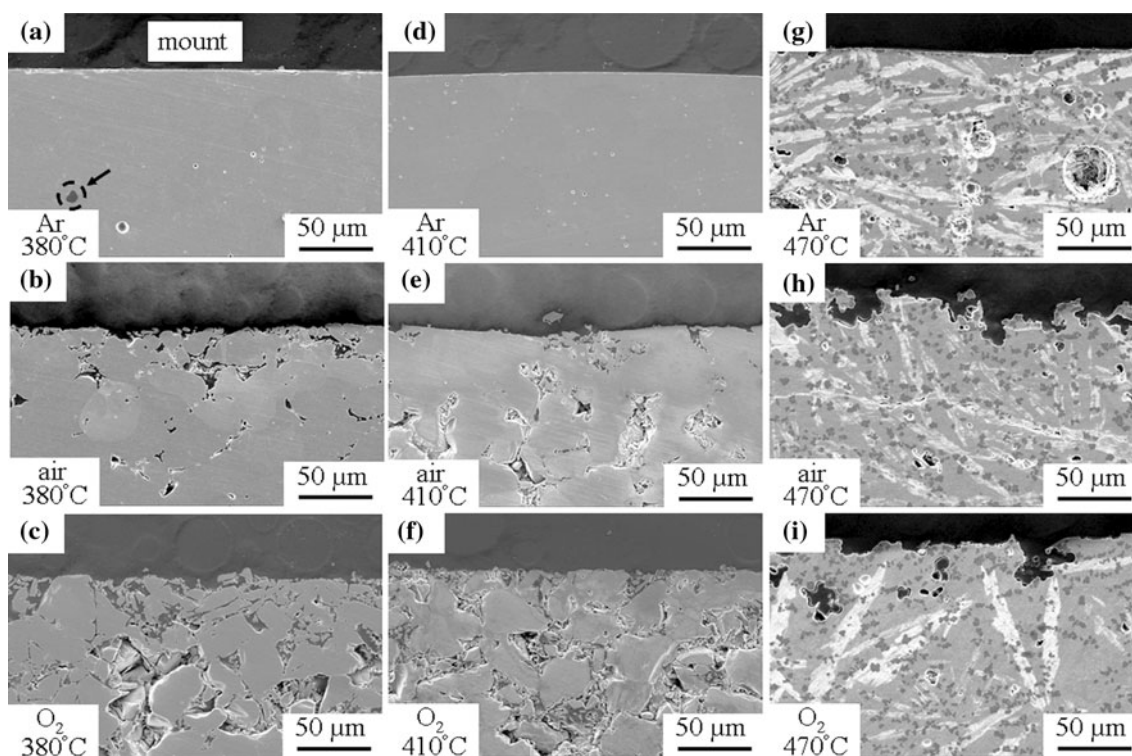
Fig. 8 Cross-sectional micrographs of the samples sintered at 380–470 °C for 20 min in various atmospheres

Table 1 Surface characteristics and water durability of the samples sintered at 380–470 °C for 20 min in various atmospheres

Sintering atmosphere	Sintering temperature (°C)										
	380				410				470		
	Crystalline phase		Porosity	DR (10^{-6} g/cm^{2}min)	Crystalline phase		Porosity	DR (10^{-6} g/cm^{2}min)	Crystalline phase		Porosity	DR (10^{-6} g/cm^{2}min)
	XRD	SEM	SEM		XRD	SEM	SEM		XRD	SEM	SEM	
Ar	A	M_xP	F.D.	0.28 ± 0.15	S_3P, M_3P	M_xP, S_3P	F.D.	0.39 ± 0.07	α-M_2P, M_3P, S_3P	M_xP, S_3P	L	1.78 ± 0.09
Air	A	A	M	0.77 ± 0.15	S_3P, M_3P	M_xP	L	0.14 ± 0.06	α-M_2P, M_3P, S_3P	M_xP, S_3P	M	0.38 ± 0.57
O$_2$	A	A	H	0.99 ± 0.32	S_3P, M_3P	A	H	2.06 ± 0.41	α-M_2P	M_xP	H	-0.18 ± 0.12

A amorphous, *H* high, *M* middle, *L* low, *F.D.* fully densified, α-M_2P α-Mg$_2$P$_2$O$_7$ (ICDD No. 75-1055), M_3P Mg$_3$(PO$_4$)$_2$ (ICDD No. 33-0876), M_xP α-M_2P and/or M_3P, S_3P Sn$_3$(PO$_4$)$_2$ (ICDD No. 70-0391)

continuously although the surface porosity became higher (Fig. 5g–i). It is suggested that when P_{O_2} is increased, either the obviously decreased amount of S_3P phase (Fig. 6a) or the enhanced oxidation tendency of Sn^{2+} to Sn^{4+} on the glass particle surface, which increases the average bonding strength of glass structure, leads the decreased *DR*. These findings on chemical durability indicate that the P_{O_2} level during sintering affects the porosity, phase assemblage, and the amounts of crystalline

phases on the as-sintered surface, which in turn influenced water durability.

In summary, water durability of the present SnO–MgO–P$_2$O$_5$ glass can be improved when the glass is sintered at lower temperatures (e.g., 380 and 410 °C) in Ar or air atmosphere, or at higher temperatures (e.g., 470 °C) in O$_2$ atmosphere. Moreover, although there is no direct evidences supporting the existence of Sn^{4+} (e.g., by using Mössbauer spectroscopy), according to the above-described results it
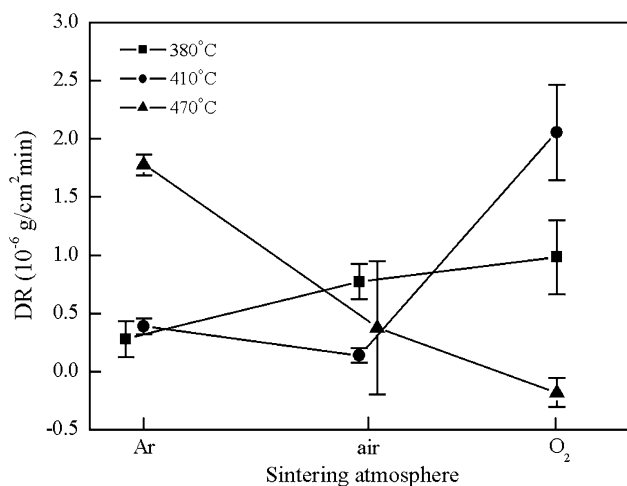
Fig. 9 Variation of the dissolution rate in 40 °C water for 540 min of the samples sintered at 380–470 °C for 20 min in various atmospheres

can be summarized that increasing P_{O_2} enhances in the oxidation tendency of Sn^{2+} to Sn^{4+}, therefore affecting the sintering, crystallization, and water durability of the SnO–MgO–P_2O_5 glass. Further investigation of Sn^{2+} oxidation is in progress using a method, e.g., secondary ion-mass spectroscopy, to examine the elemental distribution at the glass surface-region.

Conclusions

A low-viscosity stannous phosphate (SnO–MgO–P_2O_5) glass powder was sintered at 380–470 °C for 20 min under different atmospheres (Ar, air, and O_2). It was found that increasing P_{O_2} caused a greater tendency of Sn^{2+} oxidizing to Sn^{4+} on the surface of the glass particles, increasing the apparent viscosity of the glass. This increase in glass viscosity increased both the densification temperature and the crystallization temperature of the glass powder compacts, resulting in an increase in porosity and a decrease in total amount of the crystalline phases. Phase assemblage was also affected by the sintering atmosphere. The crystalline phases formed in the sintered samples are $Mg_3(PO_4)_2$, α-$Mg_2P_2O_7$, and $Sn_3(PO_4)_2$, depended on the sintering conditions (temperature and atmosphere). The P_{O_2}-dependent porosity, phase assemblage, and the amounts of crystalline phases of the as-sintered surface determined the water durability of the sintered glass. It is shown that the water durability of the sintered glass can be improved using Ar or air atmospheres for lower sintering temperatures (e.g., 380 and 410 °C) and using O_2 atmosphere for higher sintering temperatures (e.g., 470 °C).

References

1. Liang W, Cheng J (2001) Am Ceram Soc Bull 80:62
2. Campbell JH, Suratwala TI (2000) J Non-Cryst Solids 263–264:318
3. Takebe H, Nonaka W, Kubo T, Cha J, Kuwabara M (2007) J Phys Chem Solids 68:983
4. Day DE, Wu Z, Ray CS, Hrma P (1998) J Non-Cryst Solids 241:1
5. Brow RK (2000) J Non-Cryst Solids 263–264:1
6. Morena R (2000) J Non-Cryst Solids 263–264:382
7. Brow RK, Tallant DR (1997) J Non-Cryst Solids 222:396
8. Morinaga K, Fujino S (2001) J Non-Cryst Solids 282:118
9. Shaw CM, Shelby JE (1988) Phys Chem Glasses 29:49
10. Bunker BC, Arnold GW, Rajaram M, Day DE (1987) J Am Ceram Soc 70:425
11. Marino AE, Arrasmith SR, Gregg LL, Jacobs SD, Chen G, Duc Y (2001) J Non-Cryst Solids 289:37
12. Peng YB, Day DE (1991) Glass Technol 32:166
13. Shih PY (2002) J Mater Sci Lett 21:1153
14. Tick PA (1984) Phys Chem Glasses 25:149
15. Pascual L, Durán A (1996) Mater Res Bull 31:77
16. Sauze AL, Marchand R (2000) J Non-Cryst Solids 263–264:285
17. Yung H, Shih PY, Liu HS, Chin TS (1997) J Am Ceram Soc 80:2213
18. Donald IW (1993) J Mater Sci 28:2841. doi:10.1007/BF01117591
19. Shaw CM, Shelby JE (1988) J Am Ceram Soc 71:252
20. Shih PY, Yung SW, Chen CY, Liu HS, Chin TS (1997) Mater Chem Phys 50:63
21. Ding JY, Shih PY, Yung SW, Hsu KL, Chin TS (2003) Mater Chem Phys 82:61
22. Cha J, Kubo T, Takebe H, Kuwabara M (2008) J Ceram Soc Jpn 116:915
23. Xu XJ, Day DE (1990) Phys Chem Glasses 31:183
24. Tick PA (1983) US Patent 4,379,070
25. Morena R (1996) US Patent 5,514,629
26. Morena R (1996) US Patent 5,516,733
27. Morena R (2000) US Patent 6,048,811
28. Yamanka T (2003) US Patent 6,617,269
29. Taketami K (2003) JP 2003252648
30. Shyu JJ, Yeh CH (2007) J Mater Sci 42:4772. doi:10.1007/s10853-006-0766-4
31. Shyu JJ, Yeh CH (2009) J Mater Sci 44:2985. doi:10.1007/s10853-009-3396-9
32. Sears A, Hölland D, Dowsett MG (2000) Phys Chem Glasses 41:42
33. Bekaert É, Montagne L, Delevoye L, Palavit G, Revel B (2004) C R Chimie 7:377
34. Hölland D, Smith ME, Poplett IJF, Johnson JA (2001) J Non-Cryst Solids 293–295:175
35. Nishida T, Katada M, Osawa N, Sato R, Komatsu T, Matusita K (1994) Hyper Interact 94:2119
36. Bhat MH, Berry FJ, Jiang JZ, Rao KJ (2001) J Non-Cryst Solids 291:93
37. Bekaert É, Montagne L, Delevoye L, Palavit G, Wattiaux A (2004) J Non-Cryst Solids 345–346:70
38. Williams KFE, Johnson CE, Nikolov O, Thomas MF, Johnson JA, Greengrass J (1998) J Non-Cryst Solids 242:183

39. Williams KFE, Johnson CE, Greengrass J, Tilley BP, Gelder D, Johnson JA (1997) J. Non-Cryst Solids 211:164

40. Takeda S, Akiyama R, Hosono H (2001) J Non-Cryst Solids 281:1

41. Principi G, Maddalena A, Gupta A, Geotti-Bianchini F, Hreglich S, Verità M (1993) Nucl Instrum Methods Phys Res B76:215

42. Ehrt D (2008) J Non-Cryst Solids 354:546

43. Muñoz F, Pascual L, Durán A, Rocherullé J, Marchand R (2006) J Eur Ceram Soc 26:1455

44. Kingery WD, Bowen HK, Uhlmann DR (1976) Introduction to ceramics, 2nd edn. Wiley, New York, p 492

45. Berry FJ, Thied RC (1997) J Alloys Compd 257:201